Regular Article

PHYSICAL CHEMISTRY RESEARCH
Published by the
Iranian Chemical Society
www.physchemres.org
info@physchemres.org

***Phys. Chem. Res.**, Vol. 7, No. 1, 65-80, March 2019*
DOI: 10.22036/pcr.2018.147945.1537

Codeposition of Fe_3O_4 Nanoparticles Sandwiched Between g-C_3N_4 and TiO_2 Nanosheets: Structure, Characterization and High Photocatalytic Activity for Efficiently Degradation of Dye Pollutants

Z. Abbasi[a], A. Farrokhnia[a,*], E.I. Garcı´a-Lo´pez[b] and M. Zargar Shoushtari[c]

[a]*Department of Chemistry, Faculty of Science, Shahid Chamran University of Ahvaz, Ahvaz, Iran*

[b]*''Schiavello-Grillone'' Photocatalysis Group, Dipartimento di Energia, Ingegneria dell'informazione e modelli Matematici (DEIM), Universita` di Palermo, Viale delle Scienze, 90128 Palermo, Italy*

[c]*Department of Physics, Faculty of Science, Shahid Chamran University of Ahvaz, Ahvaz, Iran*

(Received 8 September 2018, Accepted 29 November 2018)

Novel ternary nanocomposite photocatalysts based on g-C_3N_4/Fe_3O_4/TiO_2 nanosheet were synthesized using simple solid combustion, hydrothermal and wetness impregnation methods. The g-C_3N_4 nanosheet (2D)/ Fe_3O_4/TiO_2 nanosheet (2D) triad-interface nanocomposite arranged in the form of Fe_3O_4 nanoparticle was sandwiched and effectively dispersed on the surface between g-C_3N_4 and TiO_2 nanosheets. The synthesized composites were characterized by some specific techniques such as X-ray diffraction (XRD), Fourier transform infrared (FT-IR) spectroscopy, field emission scanning electronic microscopy (FE-SEM), transmission electron microscope (TEM), vibrating sample magnetometer (VSM), specific surface area (SSA), and dynamic laser scattering (DLS) analyzer. The effect of Fe_3O_4 loading quantity on photocatalytic overall performance indicated that g-C_3N_4 nanosheets/Fe_3O_4/TiO_2 nanosheets with 5% wt Fe_3O_4 nanoparticle exhibit the best photocatalytic ability. These composites showed excellent activities in the UV-light-driven degradation of direct blue (DB), methyl blue (MB) and safranin (SA). After irradiation for 210 min, the methylene blue (MB) degradation efficiency was 63% for g-C_3N_4, 58% for TiO_2, 71% for g-C_3N_4-TiO_2, 85% for g-C_3N_4-1% wt Fe_3O_4-TiO_2, 96% for g-C_3N_4-5% wt Fe_3O_4-TiO_2 and 77% for g-C_3N_4-10% wt Fe_3O_4-TiO_2 indicating that nanocomposites with 5 wt% Fe_3O_4 had the best photocatalytic performance. The SSA of the TiO_2, g-C_3N_4, g-C_3N_4-TiO_2 and g-C_3N_4-10% wt Fe_3O_4-TiO_2 were determined using Sear's method. Finally, it is worth mentioning that the surface area of the g-C_3N_4-10% wt Fe_3O_4-TiO_2 photocatalyst has been found to be 66.2 m^2 g^{-1}.

Keywords: Heterostructure, Photocatalyst, Photocatalytic activity, Nanosheet

INTRODUCTION

In recent decades, photocatalysis has been noted to be one of the most significant advances in treating natural contamination. The photocatalysts, responding to the light, are immediately requested in the photo-catalysis technological know-how due to their expanding reaction to the daylight. In other words, the improvement will ameliorate the utilization of daylight [1]. An ideal photocatalyst should have the following characteristics: (i) being photoactive, (ii) having the capability to make use of the visible or near-UV light, (iii) being biologically and chemically inactive, (iv) having photostability quality, (v) having cheap and (vi) non-noxious [2] capacities. Semiconductor-based photocatalysts such as TiO_2, SnO_2, ZnO and WO_3 have recently received great attention due to their essential applications in explaining the worldwide environmental pollutants [3]. TiO_2 is well-known and commonly used as a semiconductor photocatalyst for the photodegradation of organic pollutants in wastewater due to its low price, high profuse, non-toxicity, safety, good stability and outstanding photocatalytic performance. Unfortunately, TiO_2 undergoes some deficiencies that effectively restricte its large-scale practical application; *e.g.*,

*Corresponding authors. E-mail: Ab.farrokhnia@scu.ac.ir

it contains a low sun power conversion efficiency and a high recombination of photogenerated electron-hole pairs due to its large band gap energy. As a result, great efforts have been made to enhance its optical absorption and the total photocatalytic performance under visible light irradiation [4]. A metal-free semiconductor, such as graphitic carbon nitride (g-C_3N_4), has recently drawn a significant attention in water splitting and photocatalytic degradation of pollutants under visible light. g-C_3N_4 is a typical metal-free polymeric semiconductor which is an extremely encouraging material for sun oriented power use. In addition, g-C_3N_4 has a high thermal and chemical stability, nontoxicity and also is simple to prepare. g-C_3n_4 has a desirable band gap of 2.7 eV [5,6].

A large number of investigations have been performed on organic dye degradation and hydrogen or oxygen generation from water splitting under visible light illumination. Besides, further properties of g-C_3N_4 are developing rapidly [7-9]. Lately, many researchers have focused on ultra-thin sheet-like nanostructures [10-13]. Chen and Mao [14] synthesized Fe_2O_3-TiO_2 composite photocatalyst with enhanced photocatalytic performance in the direction of the photodegradation of Rhodamine B (RhB) under visible-light irradiation. Shanmugam *et al.* [15] made graphene-TiO_2 composite and achieved an enhanced photocatalytic performance for the degradation of methylene blue (MB) under visible light irradiation. Weibin and co-worker [16] made TiO_2@poly-phenylene composite microspheres by sol-gel method and found it to be a good photodegradation for malachite green. The presence of poly-phenylene changes the band gap of TiO_2 composite microspheres in order to greatly improve photocatalytic performance on the degradation of malachite green (98.2%) under sun-like illumination. The photo-catalytic reusability was investigated up to five alternate cycles and the activity of microspheres retained up to 85.6% of the photodegradation ratio. In this study, the g-C_3N_4/Fe_3O_4/TiO_2 nanocomposites are prepared layer by layer, and their corresponding structures and photocatalytic performances are characterized using FE-SEM, TEM, FT-IR, SSA, DLS, XRD and magnetic properties analyses. These composites showed excellent activities in the UV-light-driven degradation of direct blue (DB), methyl blue (MB) and safranin (SA).

MATERIALS AND METHODS

Materials

Titanium n-butoxide, hydrofluoric acid, melamine ($C_3H_6N_6$), ferric chloride ($FeCl_3.6H_2O$), ferrous chloride ($FeCl_2.4H_2O$), ammonia solution, methylene blue, direct blue 1 and safranin were purchased from Aldrich company. All other chemicals were used as received without further purification.

Synthesis of 2D g-C_3N_4 Nanosheets

The g-C_3N_4 bulk was synthesized at a one-step polymerization of melamine [17]. The graphitic carbon nitride (g-C_3N_4) was provided by an ordinary thermal polymerization method. 10 g of melamine ($C_3H_6N_6$) powder was transferred to an alumina crucible. The crucible was heated to 550 °C with a rising rate of 20 °C min^{-1} and kept for two hours at the essential temperature under semi-closed environment, the furnace was then cooled naturally to room temperature. The outcome which was the bulk g-C_3N_4 with yellow colour was grounded to a fine powder.

In the next step, 1 g of bulk g-C_3N_4 powder was widely separated in 500 ml water, and then, ultrasonicated for about 10 h. The resulted suspension was centrifuged at about 7000 rpm in order to remove the residual unexfoliated g-C_3N_4. The suspension was then heated at 100 °C to obtain pale yellow coloured g-C_3N_4 nanosheets.

Synthesis of 2DTiO_2 Nanosheets

Briefly, 25 ml titanium n-butoxide and 5 ml hydrofluoric acid (48-51%) were added into the beaker while mixing for 5 min, the dispersion was transferred into a Teflon autoclave. The hydrothermal reaction was carried out for 24 h at 180 °C. Once the reaction was completed, the obtained mixture was filtered and washed with NaOH aqueous solution (0.1 M) three times until the fluoride was removed from the TiO_2 nanosheets. It was then left to dry at room temperature for 24 h.

Synthesis of Fe_3O_4 Nanoparticle

Fe_3O_4 nanoparticles were prepared through an improved chemical co-precipitation method. Firstly, $FeCl_2.4H_2O$ and $FeCl_3.6H_2O$ were dissolved into deionized water with a molar ratio of 1:2, and then, the mixed solution was stirred for 10 min. Afterwards, the $NH_3.H_2O$ aqueous solution

(30%) was added dropwise into the above solution at 60 °C. After 60 min, the colour of the solution changed from dark orange to black. This indicated the formation of Fe_3O_4 nanoparticles. The prepared Fe_3O_4 nanoparticles were magnetically separated and washed with deionized water and ethanol several times and the obtained Fe_3O_4 nanoparticles were dried at 50 °C for 18 h.

Synthesis of g-C_3N_4/Fe_3O_4 Nanocomposites

g-C_3N_4/Fe_3O_4 nanocomposites were prepared by the electrostatic self-assembly method [18]. Briefly, 200 mg of the g-C_3N_4 nanosheets were widely separated in 200 ml of deionized water by ultrasound for 120 min. Meanwhile, different amounts (1 mg, 5 mg and 10 mg) of the Fe_3O_4 nanoparticles were added into 30 ml of deionized water by ultrasound for 60 min. The suspension of Fe_3O_4 nanoparticles was added dropwise to the suspension of g-C_3N_4 under dynamic stirring. The obtained mixed suspension was covered and stirred for 24 h. At the final step, the obtained product was dried in the oven at 50 °C for 18 h.

Synthesis of g-C_3N_4/Fe_3O_4/TiO_2 Ternary Nanocomposite

To prepare the g-C_3N_4/Fe_3O_4/TiO_2 ternary nanocomposite, 100% wt of TiO_2 nanosheets (with respect to the weight of g-C_3N_4 nanosheets) were mixed in methanol/water (1:1 volume ratio) solution and ultrasonicated for 3 h. After that, the synthesized g-C_3N_4/Fe_3O_4 nanocomposite powder was added to the suspension and ultrasonicated for 120 min to form a uniform dispersion. After continuous stirring for 12 h, the final powder was obtained by centrifugation and washed with water/ethano, l and then, dried at 60 °C overnight. A series of g-C_3N_4/Fe_3O_4/TiO_2 ternary nanocomposites with 1, 5 and 10% wt Fe_3O_4 into g-C_3N_4 were synthesized and denoted as g-C_3N_4/Fe_3O_4 (1% wt)/TiO_2, g-C_3N_4/Fe_3O_4 (5% wt)/TiO_2 and g-C_3N_4/Fe_3O_4 (10% wt)/ TiO_2, respectively.

Characterization

A field emission scanning electron microscope (FESEM, MIRA3TESCAN-XMU) was used to characterize the morphologies of all the synthesized samples. The appearance of the magnetic nanoparticles was observed by the LEO 906 E transmission electron microscope (TEM, Germany). The crystal phases of the sample were analyzed using X-ray diffractometer (XRD) with radiation (l = 0.154178 nm). A scan rate of 0.11 s^{-1} was applied to record the powder XRD patterns for 2θ in the range of 10-70°.

The Fourier transform infrared (FT-IR) spectra of the as-synthesized photocatalysts were obtained at room temperature, using a Shimadzu FTIR-8300 spectrophotometer with 4 cm^{-1} resolution. The measured absorbance was taken by UV-Vis spectrophotometer (Cintra 101 GBC Scientific Equipment Ltd.). The magnetization curve was obtained using a vibrating sample magnetometer (VSM; VersaLabTM3T cryogen-free VSM) under a magnetic field from -15,000 to 15,000 Oe.

The volume-average diameter and size distribution of the samples were measured by DLS.NanoZS (red badge) ZEN 3600.

Specific surface area (SSA) of the photocatalyst composites was estimated according to Sear's method [19]. The sample of the powdered photocatalyst (0.5 g) was acidified with 0.01 M HCl to a pH = 3. The volume was made up to 50 ml with distilled water after the addition of 10.0 g of NaCl. The solution was titrated with standard 0.01 M NaOH and the volume (V) was required to raise the pH from 4.0 to 9.0. Specific surface areas of the synthesized photocatalyst were computed from Eq. (1):

$$SSA\ (m^2\ g^{-1}) = 32V - 25 \quad (1)$$

V stands for the volume of NaOH needed to increase the pH of the sample from 4-9.

MB (10 ppm), DB (15 ppm) and SA (6 ppm) were chosen as model dye pollutants to evaluate the photocatalytic activity of the as-prepared layer by layer structured catalysts. Artificial irradiation was provided by 30W (UV-C) mercury lamp (Philips, Holland).

For each photodegradation test, a photocatalyst (5 mg) was added into 50 ml of the dye solution in a 100 ml beaker. Prior to UV light irradiation, the reaction mixture was mechanically stirred for 20 min in the dark to ensure the adsorption-desorption equilibrium. Then, the reaction mixture was exposed to UV radiation. At a fixed time

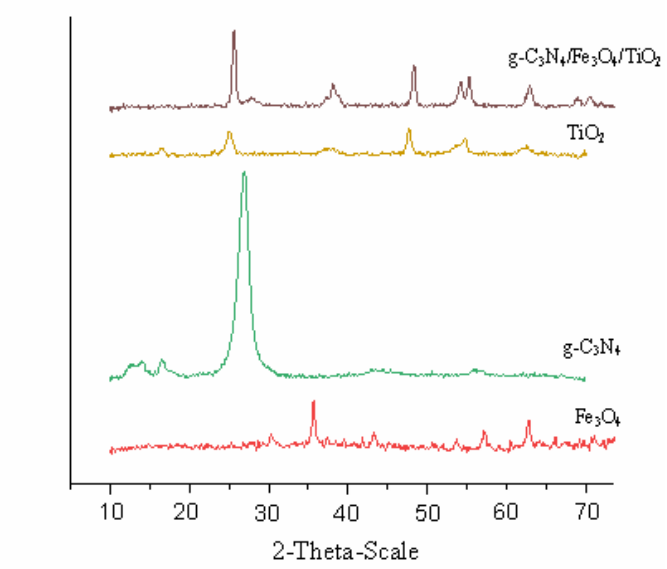

Fig. 1. TheXRD patterns for g-C_3N_4, Fe_3O_4, TiO_2 and g-C_3N_4/Fe_3O_4/TiO_2 nanocomposite.

interval, 5 ml of suspension was sampled and centrifuged in order to separate and remove the catalyst. Subsequently, the absorbance of dyes solution was recorded using a UV-Vis spectrophotometer at 662 nm, 618 nm and 518 nm which is the maximum absorption wavelength of MB, DB and SA, respectively. The progress in photocatalytic degradation of the aqueous solution was calculated using the following equation: $C_t/C_0 = A_t/A_0$, where C_0 and C_t are the initial and real-time concentrations of the dyes solution. A_0 and A_t represent the initial and real-time absorbances of dye solutions.

RESULTS AND DISCUSSION

The purity of the prepared g-C_3N_4, Fe_3O_4, TiO_2 and g-C_3N_4/Fe_3O_4/TiO_2 nanocomposites were examined using X-ray diffraction. The XRD pattern of the powders is shown in Fig. 1.

The XRD pattern presents peaks corresponding to Fe_3O_4, indices (220), (311), (400), (422), (511) and (440) diffraction planes, which are similar to those reported for Fe_3O_4 nanoparticles [18]. The results confirmed that anatase phase TiO_2 was successfully synthesized through the one-step hydrothermal method. TiO_2 nanosheets with a large and well exposed (001) diffraction plane were successfully synthesized. This is very critical for photocatalytic reactions because the (001) plane is the most active plane for photocatalysis [20]. The peaks of g-C_3N_4 at 27.2° and 12.8° can be indexed as (002), (100) diffraction planes, respectively. The XRD pattern of in g-C_3N_4/Fe_3O_4/TiO_2 indicates that the peaks of Fe_3O_4 crystal phase can be found at 2θ = 30.2°, 35.5°, 43.2°, 53.4°, 57.3° and 62.6°. It is It is worth noting that the diffraction peak position at 27.2° in the g-C_3N_4/Fe_3O_4/TiO_2 pattern is lower than the g-C3N4 pattern, which may result from might be due to the restricted restraining the stacking of g-C_3N_4 perpendicular to the (002) direction due to introducing TiO_2 and Fe_3O_4. This is an improve the increasing dispersity and the specific surface area of g-C_3N_4 that was observed to have a better photocatalytic activity [21].

The FT-IR spectra of the Fe_3O_4, pure TiO_2, pure g-C_3N_4 and g-C_3N_4/Fe_3O_4/TiO_2 composite are shown in Fig. 2. The results show that the peak at 807 cm^{-1} was related to the characteristic breathing mode of triazine units and strong absorption bands. The peaks at 1254 cm^{-1}, 1313 cm^{-1}, 1416 cm^{-1}, 1580 cm^{-1} and 1642 cm^{-1} correspond to the typical stretching modes and to the aromatic C-N heterocycles of g-C_3N_4 [21]. Furthermore, the wideband at 3000-3250 cm^{-1} could be referred to the stretching vibration of N-H. Infrared studies indicated the presence of a strong absorption line in both the coated and pure magnetite located at 563 cm^{-1} which was attributed to the stretching vibration of Fe-O sites. One of the outstanding peak bands occurred at 664

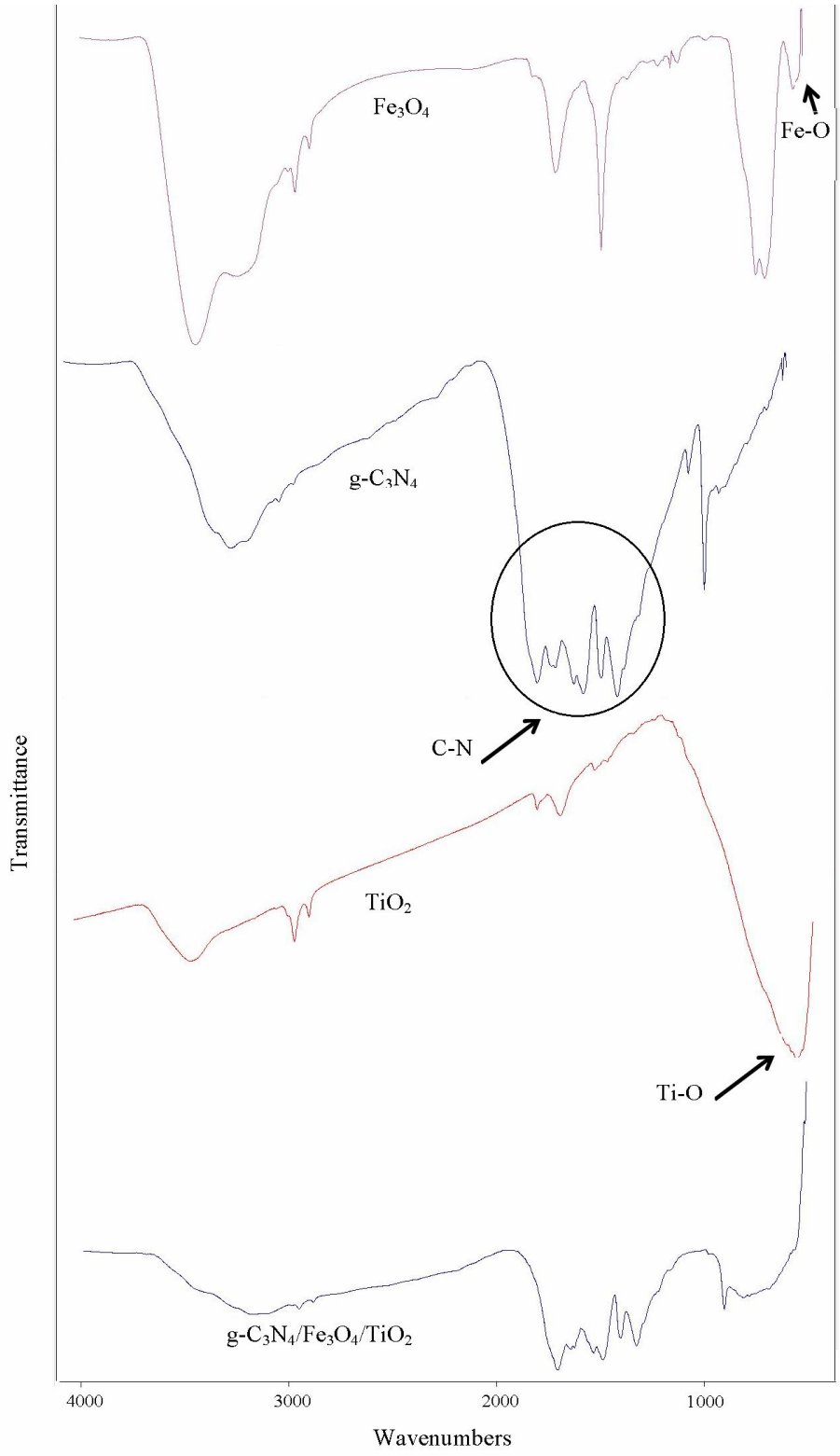

Fig. 2. The FT-IR spectra for the g-C_3N_4, Fe_3O_4, TiO_2 and g-C_3N_4/Fe_3O_4/TiO_2 nanocomposite.

cm^{-1} was the symmetric stretching of oxygen atoms along Fe-O bonds [21]. The pure TiO_2 represented a wide absorption peak at 400-700 cm^{-1} which corresponded to the Ti-O stretching and Ti-O-Ti bridging and stretching modes [4]. The peaks shown at 1630 and 3406 $cm^{-1}$are assigned to the bending of the H-O-H molecules and the O-H stretching vibration, respectively. The results of FT-IR led us to conclude that the ternary facet coupled heterojunctions contained the structure of g-C_3N_4, Fe_3O_4 and TiO_2. These functional groups of each component were contained without destruction.

To study the structure of the synthesized samples, FESEM measurements were carried out as illustrated in Fig. 3. The FESEM image of the pure TiO_2 showed small planes like nanosheets and pure g-C_3N_4 appeared as thin layers containing a nanosheet like structure.

As shown in Fig. 3a and b, these nanosheets with uniformly ultrathin 2D-structures were connected and, even across FESEM and TEM analysis, carried out to investigate the surface morphology of pure TiO_2, pure g-C_3N_4 and g-C_3N_4/Fe_3O_4/TiO_2nanocomposites. Similarly, the FESEM studies of g-C_3N_4/TiO_2 composite showed the small TiO_2 nanosheets attached to the sheet-like structure of g-C_3N_4. Compared to pure TiO_2 and pure g-C_3N_4 nanosheets, g-C_3N_4/Fe_3O_4/TiO_2 composite had a larger porosity, which was favourable for adsorption of the dye. However, under TEM (Fig. 3), in contrast to the very thin g-C_3N_4 nanosheets, TiO_2 nanosheets became clearly visible. Fe_3O_4 nanoparticles were visible between g-C_3N_4 and TiO_2. Figure 4 shows a graph of Fe_3O_4 and g-C_3N_4/Fe_3O_4/TiO_2. It is worth noting that the size distribution was 5.75 nm and 6.5 µm for Fe_3O_4 and g-C_3N_4/Fe_3O_4/TiO_2, respectively.

The magnetic field was cycled between -15000 and 15000 Oe and, as a result, zero coercively was obtained indicating the superparamagnetic properties. Moreover, Fig. 5a describes that the saturation magnetization (Ms) of Fe_3O_4 with the diameter of about 6 nm is 60 emu g^{-1}. The value of g-C_3N_4/Fe_3O_4/TiO_2 was reduced to 0.1 emu g^{-1} due to the formation of layered structures. In Fig. 6b, we can indicate the diamagnetic contribution of g-C_3N_4 and TiO_2 surrounding the Fe_3O_4 magnetic core particles.

The SSA of the synthesized TiO_2, g-C_3N_4, g-C_3N_4/Fe_3O_4/TiO_2 composites and silica were determined using Sear's method as discussed in Section 3. The results presented in Table 1 illustrate that the SSA of g-C_3N_4-5wt% Fe_3O_4-TiO_2 was found to be 66.2 m^2 g^{-1}. The layered surfaces of g-C_3N_4 nanosheet are covered with TiO_2 nanosheets. These nanosheets with uniformly ultrathin 2D-structure are connected to form-the sheet-like networks vertically aligned on the g-C_3N_4nanosheet surface. Codeposition of Fe_3O_4 nanoparticle sandwiched between g-C_3N_4 and TiO_2 nanosheets nanocomposite shows much higher specific-surface-area than the general sheet-like structure for pure g-C_3N_4 (11.8 m^2 g^{-1}) and pure TiO_2 (39 m^2 g^{-1}), thereby providing more active sites for the photocatalytic reaction.

The activity of the photocatalyst samples was examed, using g-C_3N_4/Fe_3O_4 (5% wt)/TiO_2, in order to investigate the degradation course of MB, DB and SA. The results are shown in Fig. 6a-c. It can be seen that after irradiating the reaction slurry with UV light, there is a gradual decrease in the absorption peaks at 662 nm, 618 nm and 518 nm, which are the maximum absorption wavelengths of MB, DB and SA, respectively. The percentage of dye degradation g was calculated by

$$D\% = \frac{C_0 - C_t}{C_0} \times 100$$

where C_0 is the initial concentration of the dye, and C_t is the time-dependent concentration [22].

As depicted in Fig. 7, plots of MB, the maximum absorption peaks at 662 nm, were gradually diminished. The peaks decreased under UV light irradiation for 210 min in the presence of the pure g-C_3N_4, pure TiO_2, g-C_3N_4/Fe_3O_4 (1% wt)/TiO_2, g-C_3N_4/Fe_3O_4 (5% wt)/TiO_2 and g-C_3N_4/Fe_3O_4 (10% wt)/TiO_2 nanocatalysts. Meanwhile, they changed the color of the solution gradually, suggesting that the structure of MB was decomposed. In addition, blank experiments in the absence of irradiation with the photocatalyst or in the presence of irradiation without the photocatalyst, similar to experiments with pure g-C_3N_4 and TiO_2 samples, were carried out to rationalize the photocatalytic activity of the as-synthesized g-C_3N_4/Fe_3O_4/TiO_2 photocatalyst.

It can be noted that the photocatalytic efficiency of g-C_3N_4/Fe_3O_4/TiO_2 gradually increased with the Fe_3O_4 loading value. However, the photoactivity for g-C_3N_4/Fe_3O_4/TiO_2 decreased with further increasein the Fe_3O_4 loading value.

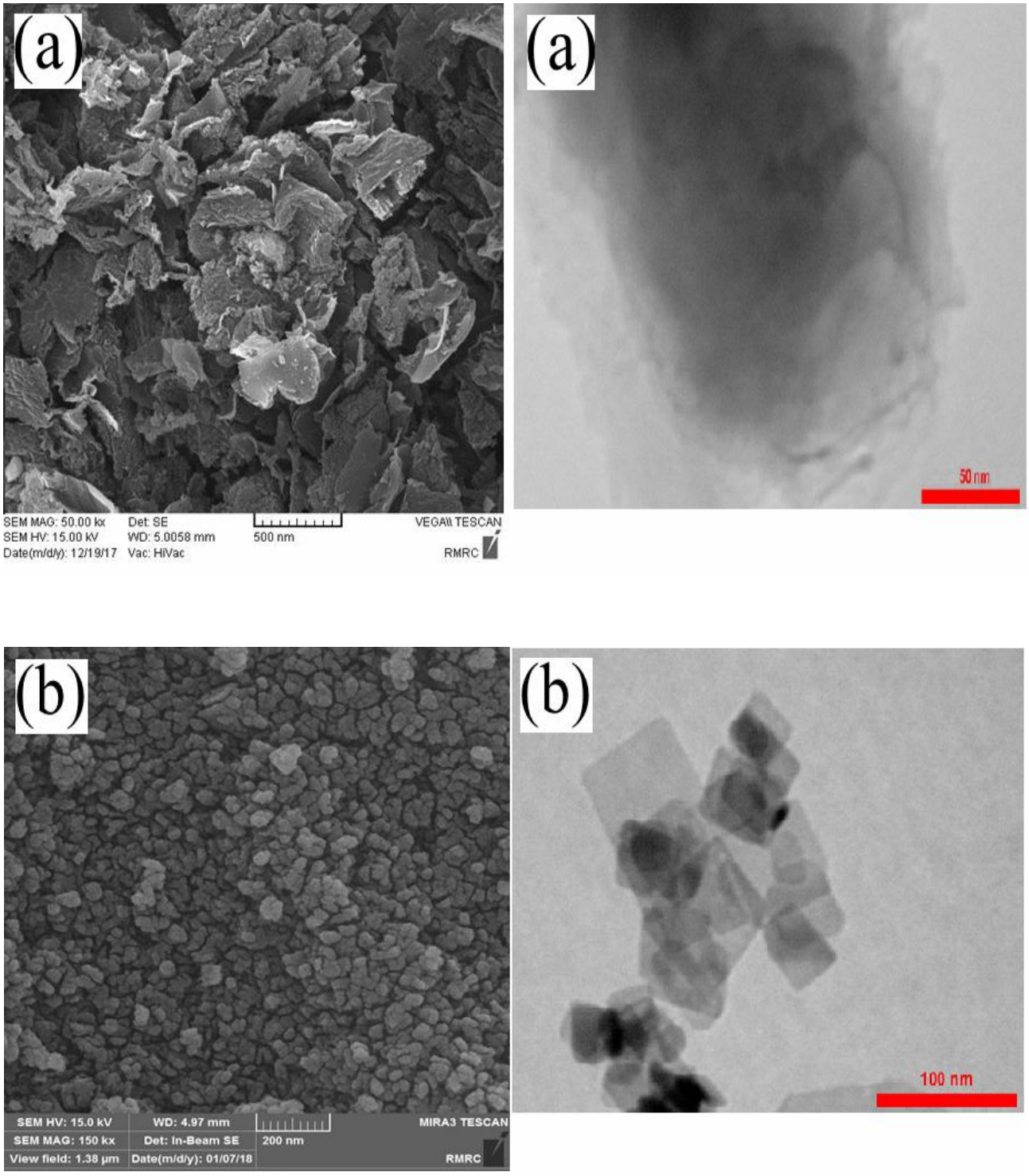

Fig. 3. The TEM and FESEM images for the (a) g-C_3N_4, (b) TiO_2 (c) Fe_3O_4 and (d) g-C_3N_4/Fe_3O_4/TiO_2 nanocomposite.

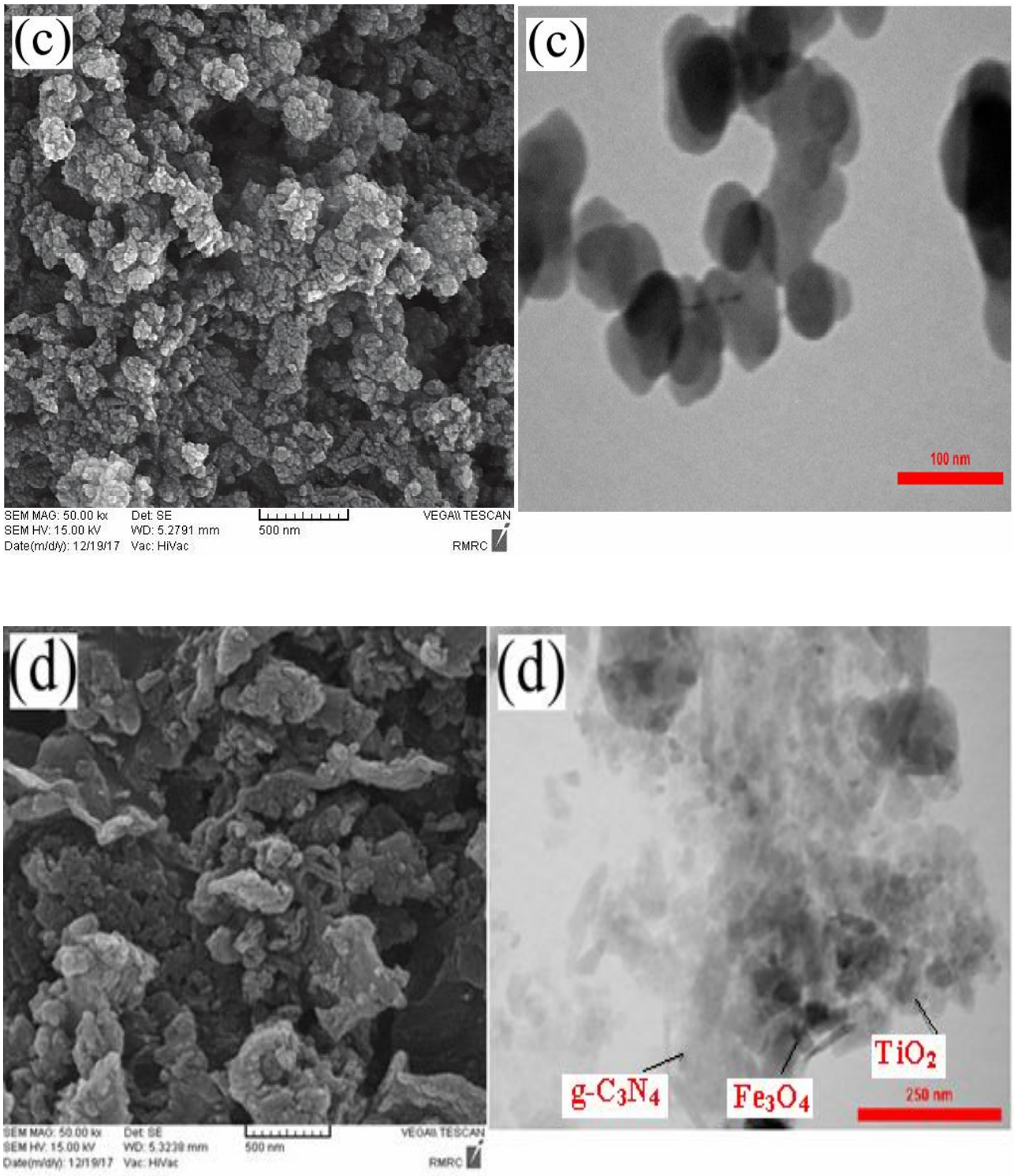

Fig. 3. Continued.

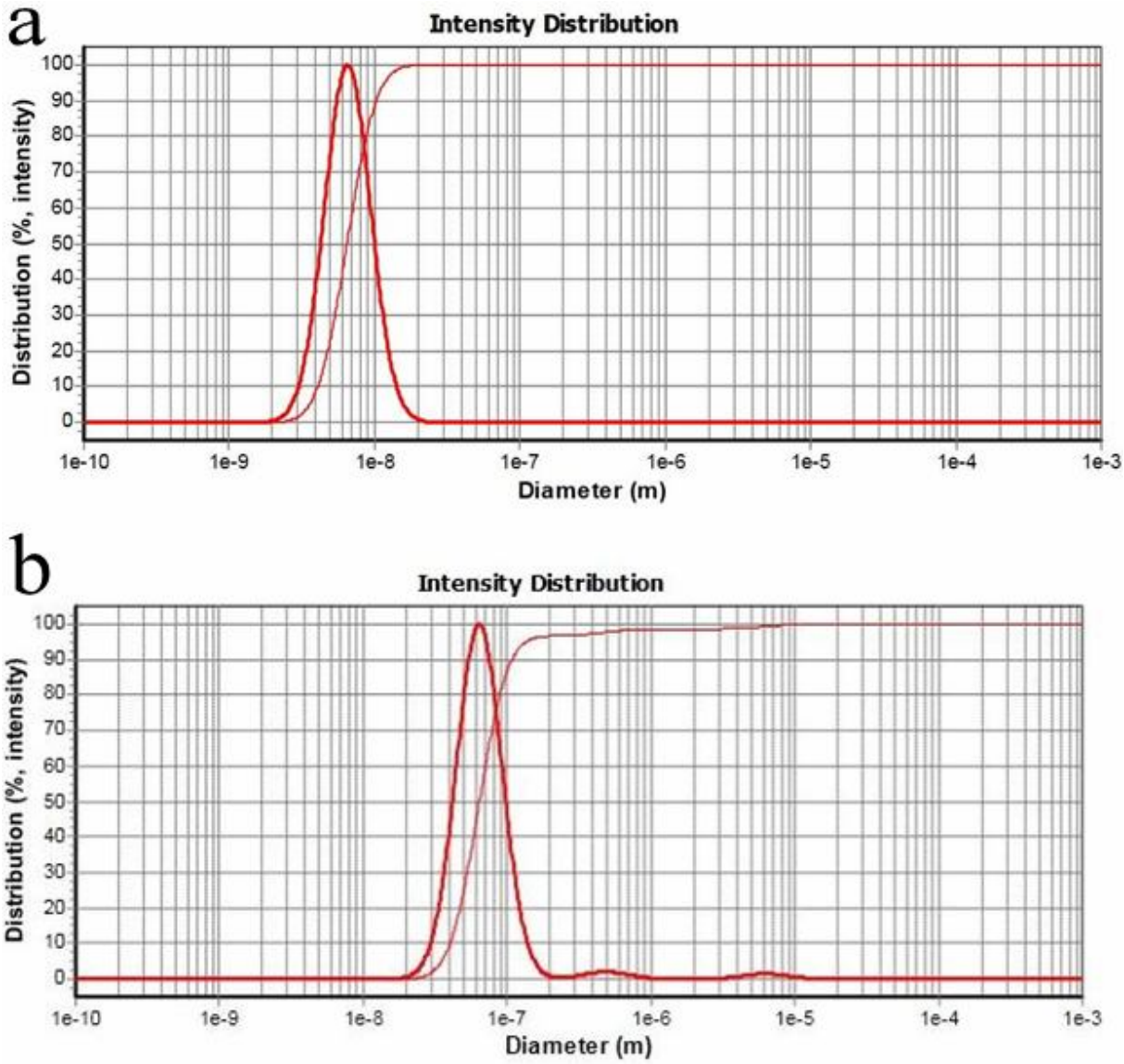

Fig. 4. The DLS spectra for size distribution of (a) Fe_3O_4 and (b) g-C_3N_4/Fe_3O_4/TiO_2 nanocomposite.

The optimum Fe_3O_4 loading value is 5% wt and g-C_3N_4/Fe_3O_4/TiO_2 is illustrating the highest degradation rate of about 96% at 210 min among all microspheres.

It is clearly evident that during the degradation reactions, the intensity of the absorption peaks gradually hase been decreased, while there were minimal changes in the peaks position. An obvious synergistic mechanism was found in the photocatalytic results shown in Fig. 8. Under UV light illumination, TiO_2 and g-C_3N_4 were energized, besides, they produced an electron-hole combination. Thus, more compelling photo-induced electrons and holes obtain an improvement in the photo-degradation procedure, with the improved photocatalytic action. With the purpose of determining the constant photocatalytic degradationrate, an attempt was made to fit the data using some common kinetic equations. The first-order kinetics was observed by linear plots of $\ln(C_0/C_t)$ against the irradiation time. The kinetice Eq. (2) could be expressed as follows:

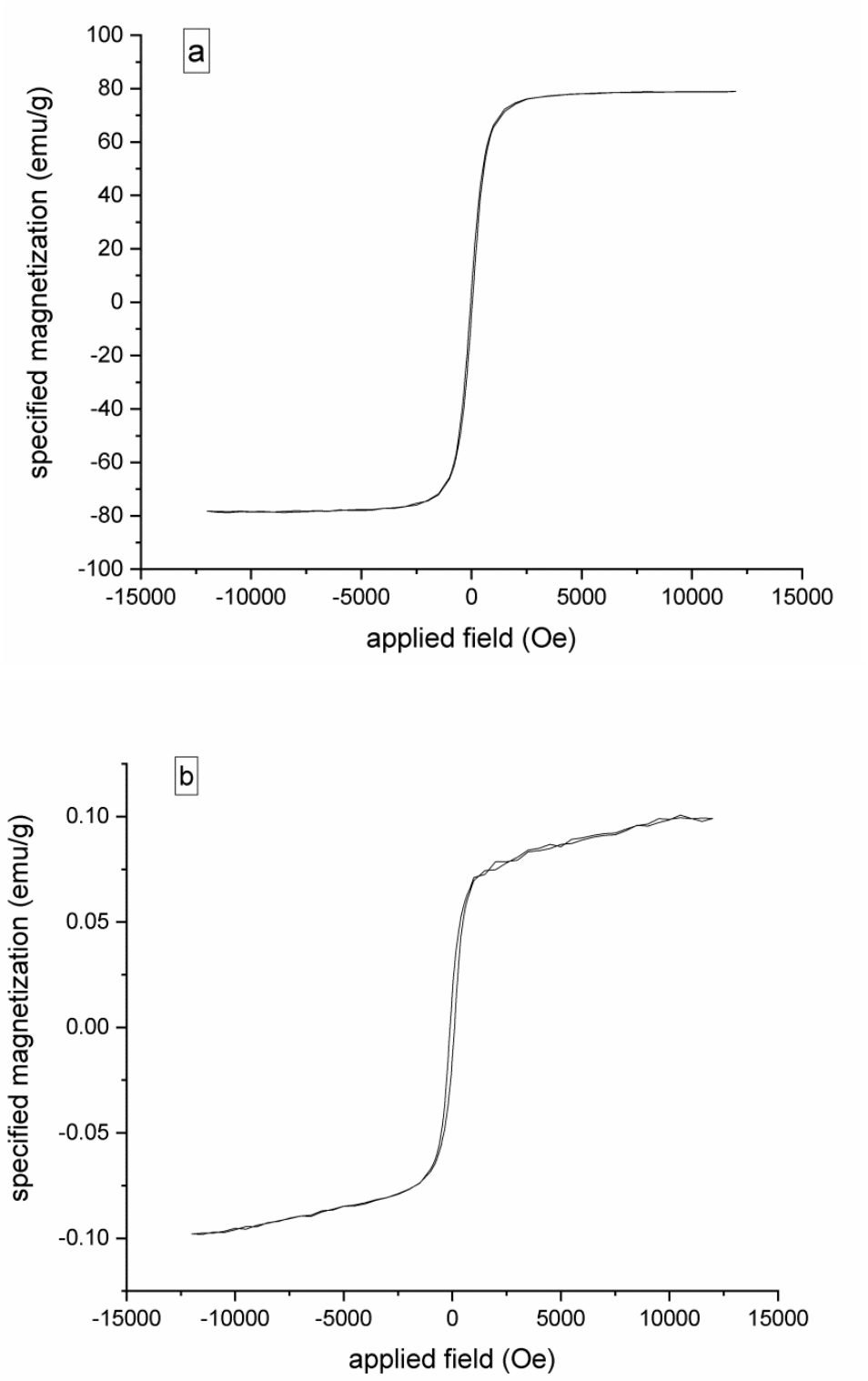

Fig. 5. The VSM curves for (a) Fe_3O_4 and (b) g-C_3N_4/Fe_3O_4/TiO_2 nanocomposite.

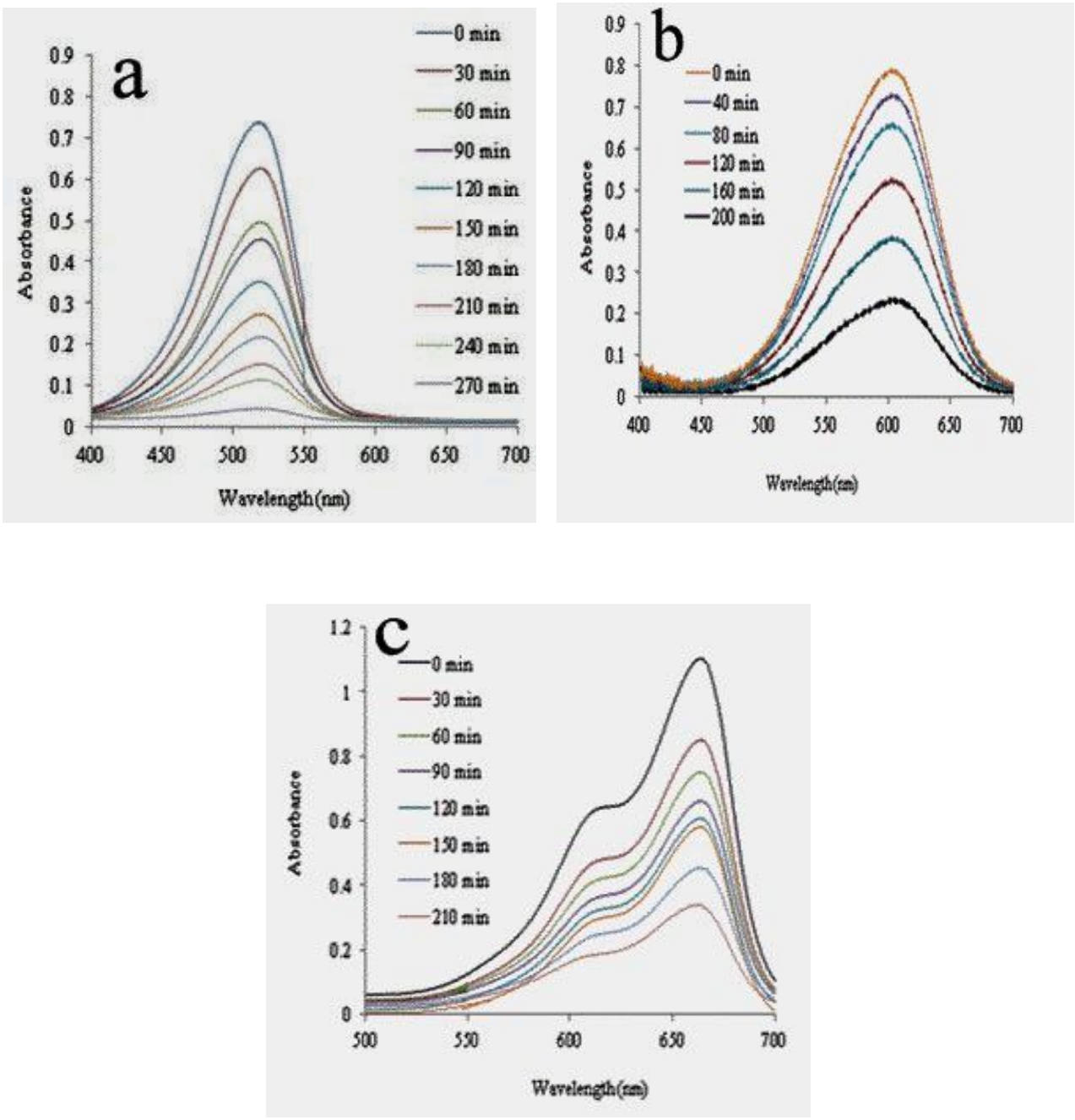

Fig. 6. The UV-Vis spectra for degradation under UV irradiation (a) SA after 270 min irradiation, (b) DB after 200 min irradiation, and (c) MB after 210 min irradiation.

$$\ln \frac{C_0}{C_t} = kt \quad (2)$$

where C_0 and C_t denote the concentrations of the dye before illumination and after a certain illumination time period, respectively, k is the first-order rate constant and t is the illumination time. The observed first-order rate constants of

Table 1. SSA of g-C_3N_4, TiO_2 and g-C_3N_4-5% wt Fe_3O_4-TiO_2

Sample	SSA (m^2 g^{-1})
g-C_3N_4	11.8
TiO_2	39
g-C_3N_4/Fe_3O_4 (5% wt)/TiO_2	66.2

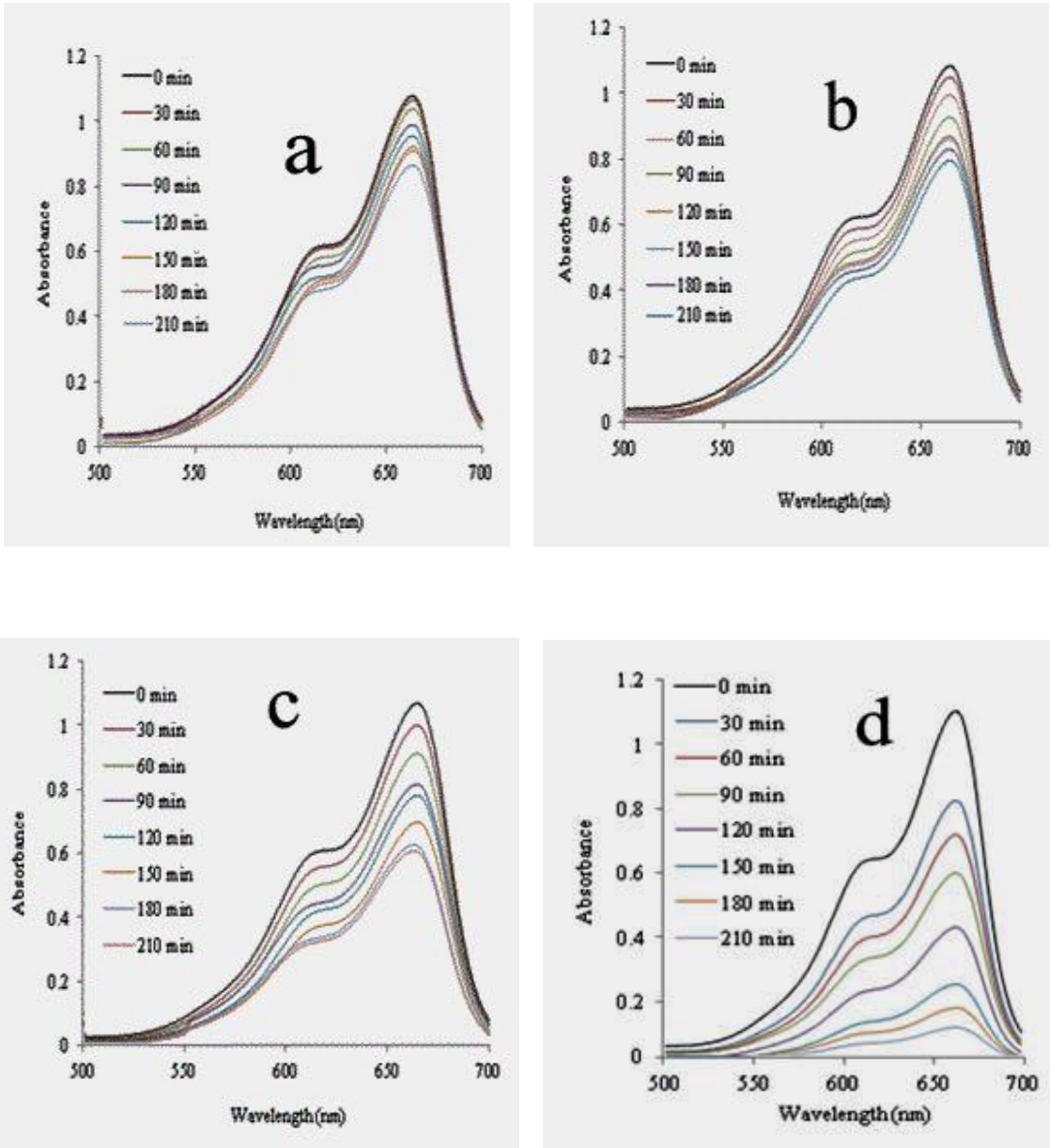

Fig. 7. Changes of MB absorbance: (a) TiO_2, (b) g-C_3N_4, (c) g-C_3N_4/TiO_2, (d) g-C_3N_4/Fe_3O_4 (1% wt)/TiO_2, (e) g-C_3N_4/Fe_3O_4 (5% wt)/TiO_2, (f) g-C_3N_4/Fe_3O_4 (10% wt)/TiO_2.

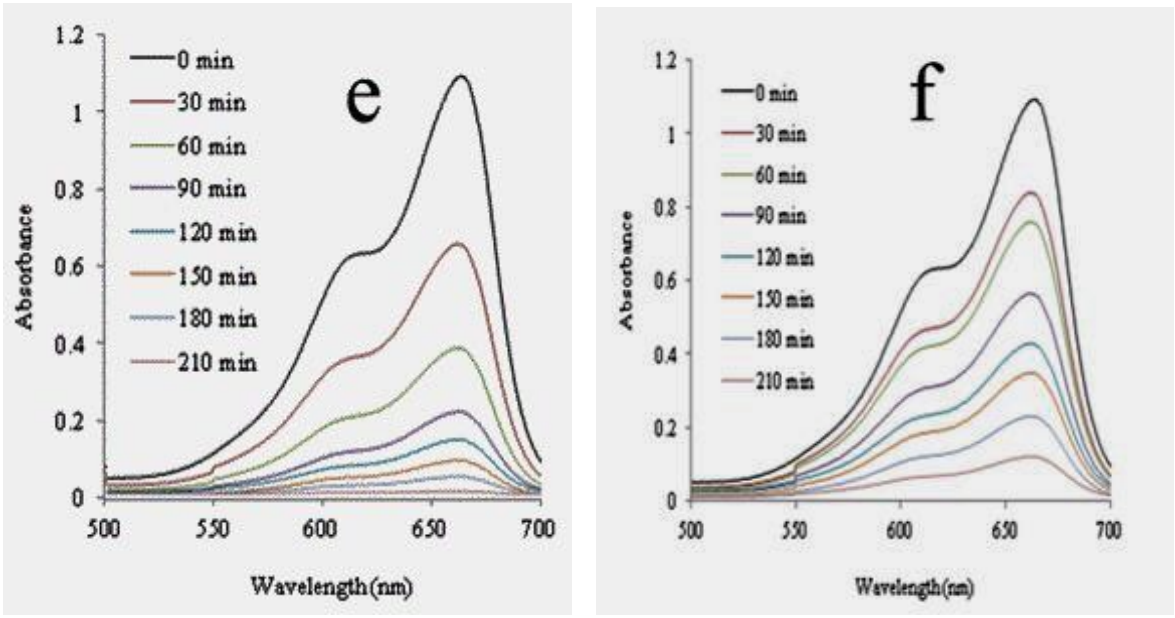

Fig. 7. Continued.

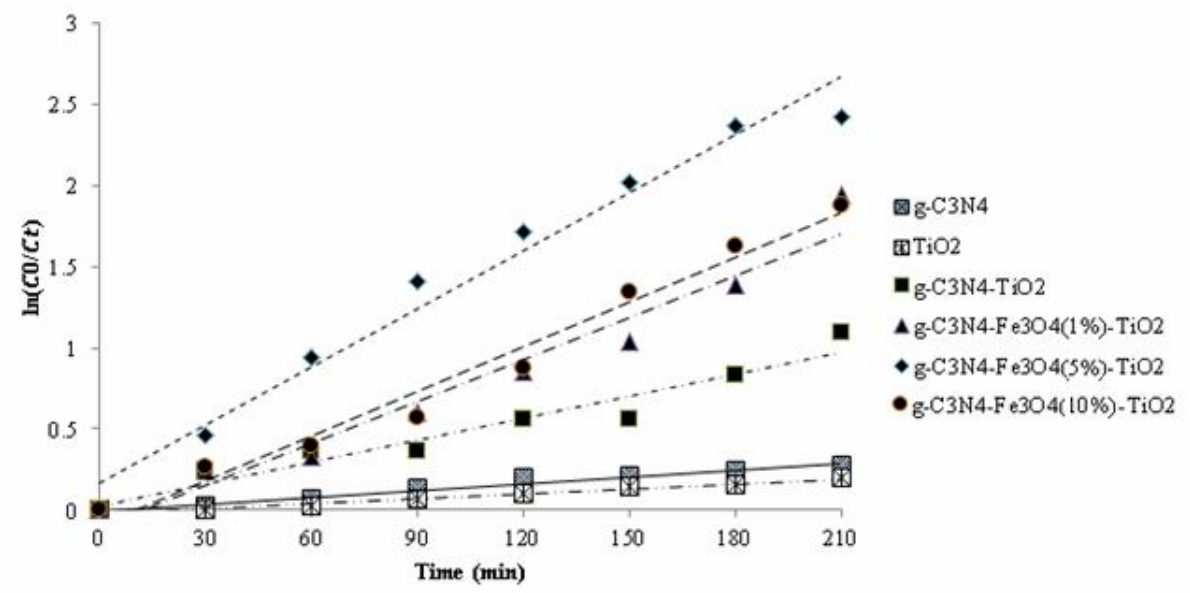

Fig. 8. The degradation rate constant of MB over different samples.

MB degradation over the samples are illustrated in Fig. 9. It was evident that the photocatalytic degradation rate constant was gradually enhanced with increasing the content of Fe_3O_4 up to 5% and then this decreased.

The rate constants for the degradation reaction over the g-C_3N_4, TiO_2, g-C_3N_4/TiO_2, g-C_3N_4/Fe_3O_4 (1% wt)/TiO_2, g-C_3N_4/Fe_3O_4 (5% wt)/TiO_2, g-C_3N_4/Fe_3O_4 (10% wt)/TiO_2 samples are 14×10^{-4}, 11×10^{-4}, 45×10^{-4}, 86×10^{-4}, $119 \times$

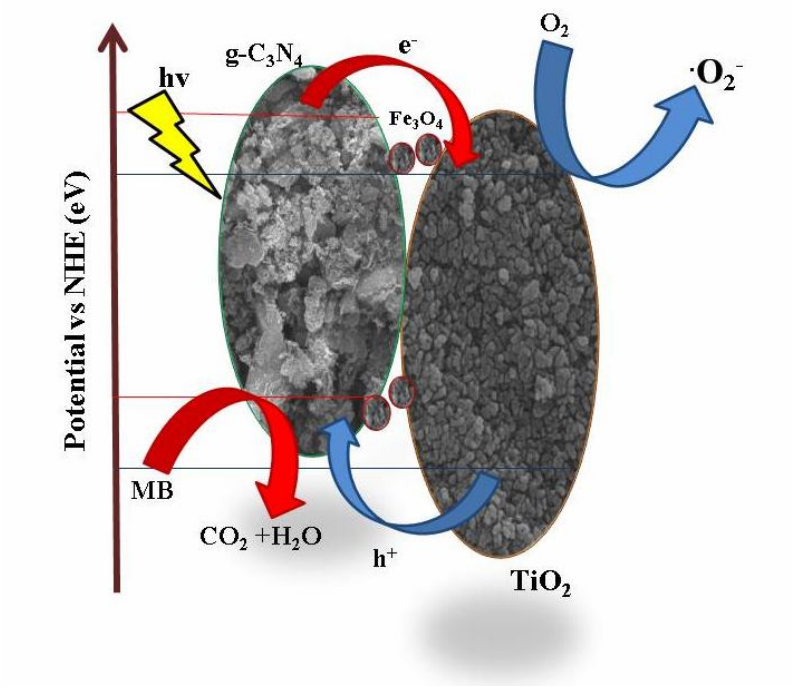

Fig. 9. Mechanism of the photocatalytic induction process in the g-C_3N_4/Fe_3O_4 (5% wt)/TiO_2 nanocomposite: visible induced mechanism and UV induced mechanism.

10^{-4} and 92 × 10^{-4} min^{-1}. Hence, photocatalytic activity of the g-C_3N_4/Fe_3O_4 (5% wt)/TiO_2 nanocomposite was nearly 1.38 and 1.29 times as high as those of the g-C_3N_4/Fe_3O_4 (1% wt)/$TiO_2$and g-C_3N_4/Fe_3O_4 (10% wt)/TiO_2 samples, respectively.

It is documented that the introduction of g-C_3N_4 into oxide semiconductors can significantly enhance the photocatalytic performance due to its relative negative CB potential (1.12 eV *vs*. NHE), which allows its photo-generated electrons to transfer more easily to the TiO_2 nanosheets under UV irradiation. The immediate result is in the improved carrier separation efficiency and the photoactivity. Thus, a synergistic mechanism between the g-C_3N_4-Fe_3O_4 and TiO_2 for the enhanced photoactivity of degradation dye using this composite was proposed, as shown in Fig. 9.

The mechanism of the photocatalytic activity of the samples under UV-light irradiation is proposed to be as follows: the position of the conduction band (CB) of g-C_3N_4 (E_{CB} = -1.12 eV *vs*. NHE) is more negative than that of TiO_2 (E_{CB} = -0.6 eV *vs*. NHE) and thus provides possibility for a directional transfer of the photogenerated electrons from g-C_3N_4 to TiO_2. Moreover, the valence band (VB) of TiO_2 (+2.62 eV *vs*. NHE) is more positive than that of g-C_3N_4 (+1.73 eV *vs*. NHE). Hence, when the g-C_3N_4/Fe_3O_4/TiO_2 nanocomposites were irradiated under UV-light, the charge carriers are generated on g-C_3N_4 and Fe_3O_4 counterparts of the nanocomposites. Then, the photogenerated electrons on CB of g-C_3N_4 which could easily transfer to the CB of TiO_2 using Fe_3O_4 nanoparticles as electron conduction bridge the holes on VB of TiO_2 will migrate to that of g-C_3N_4, achieving the separation of charge carriers in composites. Therefore, it can be supposed that combining TiO_2 with g-C_3N_4/Fe_3O_4 may result in an improved photocatalytic efficiency compared to individual g-C_3N_4 and TiO_2.

$$\text{g-}C_3N_4/Fe_3O_4/TiO_2 + hv \longrightarrow e^-_{CB}\ (\text{g-}C_3N_4 \text{ and } TiO_2) + h^+_{VB}\ (\text{g-}C_3N_4 \text{ and } TiO_2) \quad \text{(excitation process)}$$

$$e^-_{CB}\ (\text{g-}C_3N_4) + O_2 \longrightarrow {}^{\cdot}O_2^-$$

$$e^-_{CB}\ (TiO_2) + 2H^+ + O_2 \longrightarrow H_2O_2 + e^- \longrightarrow OH^{\cdot} + OH^-$$

$$\text{Dye} + {}^{\cdot}O_2^- + {}^{\cdot}OH + h_{VB}^+ \longrightarrow$$

Degradation products

CONCLUSIONS

In summary, sandwich-like g-C_3N_4 nanosheet (2D)/Fe_3O_4/TiO_2 nanosheet (2D) ternary nanocomposite photocatalysts with UV light photocatalytic performance were successfully synthesized. The photocatalytic activities of the pure TiO_2, pure g-C_3N_4 and g-C_3N_4/Fe_3O_4/TiO_2 composite photocatalysts were monitoredin the photodegradation response of MB, DB and SA aqueous solution under UV irradiation. The multilayer structural design contained a high surface able to adsorb dye on the catalyst. Besides, a Fe_3O_4 interlayer, which avoided recombining the electrons, was isolated from the surface photocatalysts and higher charge separation efficiency of the photoinduced electron–hole pairs. Among all g-C_3N_4/Fe_3O_4/TiO_2 products with different Fe_3O_4 loading amount, 5% wt photocatalyst could omit 96% of MB in aqueous solution under UV irradiation. The degradation rate constant of MB over the g-C_3N_4 nanosheet/ Fe_3O_4 (5% wt)/ TiO_2 nanosheet nanocomposite was about 10.8 and 8.5 times larger than that of TiO_2 and g-C_3N_4, respectively, for the degradation of MB.

REFERENCE

[1] Linhui, Y.; Xiaoyun, Z.; Guowei, L.; Yuantao, C.; Yu, S.; Danzhen, L., Highly efficient $Bi_2O_2CO_3$/BiOCl photocatalyst based on heterojunction with enhanced dye-sensitization under visible light. *Appl. Catal. B: Environ.,* **2016**, *187*, 301-309, DOI: 10.1016/ j.apcatb.2016.01.045.

[2] Soo, C. W.; Juan, J. C.; Lai, C. W.; Hami, S. B. A.; Yusop, R. M., Fe-doped mesoporousanatase-brookitetitania in the solar-light-induced photodegradation of reac-tive Black 5 dye. *J. Taiwan Inst. Chem. Eng.* **2016**, *68*, 153-61, DOI: 10.1016/ j.jtice.2016.08.025.

[3] Mahsa, P.; Aziz, H. Y.; Shima, R. P., Review on the criteria anticipated for the fabrication of highly efficient ZnO-based visible-light-drivenphoto catalysts. *J. Indust. Engin. Chem.,* **2018**, *62*, 1-25. DOI: 10.1016/j.jiec.2018.01.012.

[4] Senthil, R. A.; Theerthagiri, J.; Selvi, A.; Madhavan, J., Synthesis and characterization of low-cost g-C_3N_4/TiO_2 composite with enhanced photocatalytic performance under visible-light irradiation, *Optical Mater.,* **2017**, *64*; 533-539, DOI: 10.1016/ j.optmat.2017.01.025.

[5] Mitra, M.; Aziz, H. Y.; Shima, R. P., Review on magnetically separable graphitic carbon nitride-based nanocomposites as promising visible-light-driven photocatalysts, *J. Mater. Sci.: Mater. Electron.,* **2018**, *29*, 1719-1747, DOI: 10.1007/s10854-017-8166-x.

[6] Akhundi, A.; Habibi-Yangjeh, A., Ternary g-C_3N_4/ZnO/AgCl nanocomposites: Synergistic collaboration on visible-light-driven activity in photodegradation of an organic pollutant, *Appl. Surface Sci.,* **2015**, *358*, 261-269, DOI: 10.1016/ j.apsusc.2015.08.149.

[7] Xiufang, C.; Jinshui, Z.; Xianzhi, F.; Markus, A.; Xinchen, W., Fe-g-C_3N_4-catalyzed oxidation of benzene to phenol using hydrogen peroxide and visible light. *J. Am. Chem. Soc*., **2009**, *131*, 11658, DOI: 10.1021/ja903923s.

[8] Li, F. T.; Zhao, Y.; Wang, Q.; Wang, X. J.; Hao, Y. J.; Liu, R. H., Enhanced visible-light photocatalytic activity of active Al_2O_3/g-C_3N_4 heterojunctions synthesized *via* surface hydroxyl modification. *J. Hazard Mater.,* **2014**, *283*, 371-81, DOI: 10.1016/ j.jhazmat.2014.09.035.

[9] Chong, M. N.; Tneu, Z. Y.; Poh, P. E.; Jin, B.; Aryal, R., Synthesis, characterisation and application of TiO_2-zeolite nanocomposites for the advanced treatment of industrial dye wastewater. *J. Taiwan Inst. Chem. Eng.,* **2015**, *50*, 288-96, DOI: 10.1016/ j.jtice.2014.12.013.

[10] Peng, K.; Fu, L.; Ouyang, J.; Yang, H., Emerging parallel dual 2D composites: natural clay mineral hybridizing MoS2 and interfacial structure. *Adv. Funct. Mater*., **2016**, *26*, 2666-75, DOI: 10.1002/ adfm.201504942.

[11] Li, Y.; Zhan, J.; Huang, L.; Xu, H.; Li, H.; Zhang, R., Synthesis and photocatalytic activity of a bentonite/g-C_3N_4 composite. *RSC Adv.,* **2014**, *4*, 11831-9, DOI: 10.1039/C3RA46818F.

[12] Yan, S. C.; Li, Z. S.; Zou, Z. G., Photodegradation performance of g-C_3N_4 fabricated by directly heating melamine. *Langmuir ACS J. Surf. Coll*., **2009**, *25*, 10397-401, DOI: 10.1021/la900923z.

[13] Rongcheng, W.; Jiuhui, Q., Removal of azo dye from water by magnetite adsorption-Fenton oxidation, *Water Environ. Res*., **2004**, *76*, 2637-42, DOI: 10.2175/106143004X141861.

[14] Chen, X.; Mao, S. S., Titanium dioxide nanomaterials: synthesis, properties, modifications and applications. *Chem. Rev.,* **2007**, *107*, 2891, DOI: 10.1021/cr0500535.

[15] Shuangyou, B.; Kai, L.; Ping, N.; Jinhui, P.; Xu, J.; Lihong, T., Synthesis of amino-functionalization magnetic multi-metal organic framework (Fe_3O_4/MIL-101(Al0.9Fe0.1)/NH_2) for efficient removal of methyl orange from aqueous solution. *J. Taiwan. Inst. Chem. Eng.,* **2018**, 1-9, DOI: 10.1016/j.jtice.2018.03.009.

[16] Weibin, B.; Rijin, Y.; Xiao, T.; Meiqin, G.; Ningshan, L.; Qinhui, C.; Yanlian, X.; Jinhuo, L., Sunlight highly photoactive TiO_2@poly-p-phenylene composite microspheres for malachite green degradation. *J. Taiwan. Inst. Chem. Eng.,* **2018**, 1-5, DOI: 10.1016/j.enmm.2016.01.001.

[17] Surendar, T.; Santosh, K.; Yogesh, G.; Monika, B.; Satishchandra, O., g-C_3N_4 (2D)/CdS (1D)/rGO (2D) dual-interface nano-composite for excellent and stable visible light photocatalytic hydrogen generation. *Inter. J. Hydrogen Energy*, **2016**, 1-14, DOI: 10.1016/j.ijhydene.2016.11.065.

[18] Liu, C. G.; Wu, X. T.; Li, X. F.; Zhang, X. G., Synthesis of graphene-like g-C_3N_4/Fe_3O_4 nanocomposites with high photocatalytic activity and applications in drug delivery. *RSC Adv.,* **2014**, *4*, 62492-62498, DOI: 10.1039/C4RA10616D.

[19] Sears, G. W., Determination of specific surface area of colloidal silica by titration with sodium hydroxide. *Anal. Chem*., **1956**, *28*, 1981-1983, DOI: 10.1021/ac60120a048.

[20] Weilin, W.; Zhaofeng, W.; Jingjing, L.; Zhu, L.; Steven, L.; Suib, P.; Guqiao, D.; Zhengguo, Z.; Luyi, S., Single-step one-pot synthesis of TiO_2 nanosheets doped with sulfur on reduced graphene oxide with enhanced photocatalytic activity, *Scientific Reports*, **2017**, *21*, 46610, DOI: 10.1038/srep46610.

[21] Zhu, Z.; Ziyang, L.; Dandan, W.; Xu, T.; Yongsheng, Y.; Weidong, S.; Youshan, W.; Nailing, G.; Xin, Y.; Hongjun, D., Construction of high dispersed Ag/Fe_3O_4/g-C_3N_4 photocatalyst by selective photo depositionand improved photocatalytic activity, *Appl. Catal. B Environ.,* **2016**, *182*, 115-122, DOI: 10.1016/j.apcatb.2015.09.029.

[22] Akhundi, A.; Habibi-Yangjeh, A., High performance magnetically recoverable g-C_3N_4/Fe_3O_4/Ag/Ag_2SO_3 plasmonic photocatalyst for enhanced photocatalytic degradation of water pollutants, *Adv. Powder Technol.,* **2017**, *28*, 565-574, DOI: 10.1016/j.apt.2016.10.025